Reaction Pendulum Identification

January, 2025

Author:
Pawel Wiktor

Email:
pawelwiktor.kontakt@gmail.com

GitHub:
https://https://github.com/pawelwiktor-github

Table of Contents

1 Purpose of the Exercises

The purpose of the exercises was to learn methods for identifying the physical model of a reaction pendulum [1]. The task was to develop an approximate model of the object based on obtained measurements. Subsequently, an appropriate control method was to be selected, allowing smooth position control of the pendulum and stabilization in the upper position using the electric motor with a reaction wheel mounted at its end.

2 Reaction Pendulum

The reaction pendulum (reaction pendulum) is a mechanical system that uses the principle of angular momentum conservation to control rotational motion. The system consists of:

- A pendulum with a specific mass, suspended on a rotation axis. The pendulum could be a rod or any object capable of rotational motion around its axis.
- A reaction wheel, acting as a flywheel, usually driven by an electric motor that generates angular momentum.

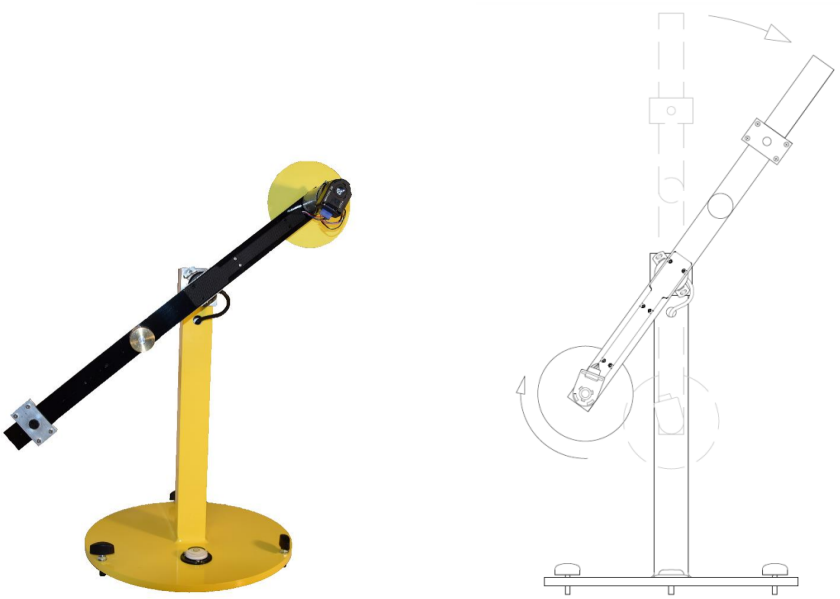

(a) Photo of RP (b) Schematic of RP

Fig. 1. Rotational Pendulum

The reaction pendulum is an unstable and nonlinear system, partially resembling an inverted pendulum. To initiate motion and maintain it in an upright position, the DC motor drives the reaction wheel forward and backward.

3 Configuration

The laboratory setup included the following tools:

- A PC with MATLAB 2018 software,
- A mechanical reaction pendulum system,
- A 12V DC motor,
- Two incremental encoders - HEDM-5505-J03,
- Power supply, power amplifiers, and signal conditioning module,
- External USB2 RT-DAC I/O board with a XILINX chip.

RP is equipped with a power interface and a universal I/O board for analog and digital signals. The system is designed for testing and verifying linear and nonlinear control algorithms. Designed algorithms in MATLAB Simulink are executed in real-time on the same PC.

The DC motor (PWM controlled) drives the flywheel, causing each change in the rotational speed of the reaction wheel to influence the angular velocity of the pendulum rod in accordance with the principle of angular momentum conservation.

4 Physics of the System

The reaction pendulum system is based on the principle of angular momentum conservation. The motion of the DC motor is possible in both directions, enabling controlled modification of torque.

5 Mathematical Model

For the reaction wheel, the structure of an inverted pendulum is initially utilized. The goal is to stabilize it at the unstable point, which is the vertical position, where the center of mass of this system is at the highest point.

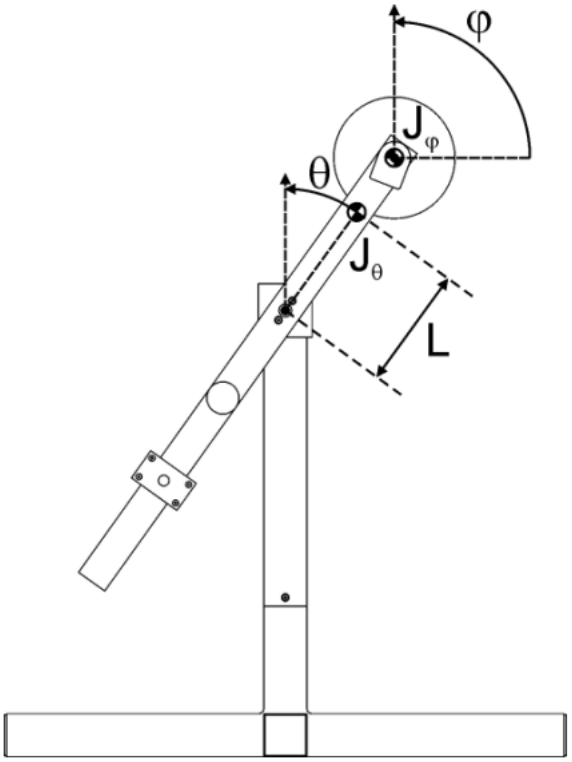

Fig. 2. Reaction pendulum model.

The physical equations describing the system are Newton's equations for rotational motion. The product of the moment of inertia and the angular acceleration of the entire pendulum is equal to the sum of individual torque forces:

$$J_\Theta \ddot{\Theta} = \sum_i M_i \tag{1}$$

where

J_Θ – Moment of inertia of the entire pendulum,
$\ddot{\Theta}$ – Angular acceleration of the entire pendulum.

Two of the torque forces are similar to the moments acting on a regular pendulum. One of them is the torque due to kinetic friction, which is the product of the friction coefficient and the angular velocity:

$$M_{\mu_\Theta} = -\mu_\Theta \dot{\Theta} \tag{2}$$

where

μ_Θ – Kinetic friction coefficient of the entire pendulum,
$\dot{\Theta}$ – Angular velocity of the entire pendulum.

The torque resulting from the weight of the entire pendulum is given by:

$$M_G = -MgLsin(\Theta) \tag{3}$$

where

MgL – Gravitational torque,
Θ – Pendulum's angular displacement.

A kinetic friction torque also acts on the system due to the rotation of the reaction wheel:

$$M_{\mu_\varphi} = -\left(\tau \frac{k_t k_r}{R} + \mu_\varphi\right) \dot{\varphi} \tag{4}$$

where

k_t – Motor constant (torque constant),
k_r – Motor constant (electric constant),
R – Motor resistance,
τ – Motor time constant,
μ_φ – Kinetic friction coefficient of the reaction wheel,
$\dot{\varphi}$ – Angular velocity of the reaction wheel.

The final torque comes from the control input:

$$M_u = \frac{k_t}{R} u \tag{5}$$

where

u – Control input.

Based on the torques and Newton's second law of motion, the following equations of motion can be derived:

$$J_\Theta \ddot{\Theta} = -MgLsin(\Theta) - \mu_\Theta \dot{\Theta} + \left(\tau \frac{k_t k_r}{R} + \mu_\varphi\right) \dot{\varphi} - \frac{k_t}{R} u \tag{6}$$

and

$$J_\varphi \ddot{\varphi} = -\left(\tau \frac{k_t k_r}{R} + \mu_\varphi\right) \dot{\varphi} + \frac{k_t}{R} u \tag{7}$$

State variables are then defined as:

$$\begin{cases} x_1 = \theta \\ x_2 = \theta' \\ x_3 = \varphi \\ x_4 = \varphi' \end{cases} \tag{8}$$

with the state equations:

$$\begin{cases} {x_1}' = x_2 \\ {x_2}' = \dfrac{1}{J_\Theta}\left(-MgL\sin(\Theta) - \mu_\Theta x_2 + \left(\tau \dfrac{k_t k_r}{R} + \mu_\varphi\right) x_4 - \dfrac{k_t}{R} u\right) \\ {x_3}' = x_4 \\ {x_4}' = \dfrac{1}{J_\varphi}\left(-\left(\tau \dfrac{k_t k_r}{R} + \mu_\varphi\right) x_4 + \dfrac{k_t}{R} u\right) \end{cases} \tag{9}$$

6 Measurements of the Real Object

Measurements of mass and distances of the real object were performed. The results are listed in Table 6 and Figure 3.

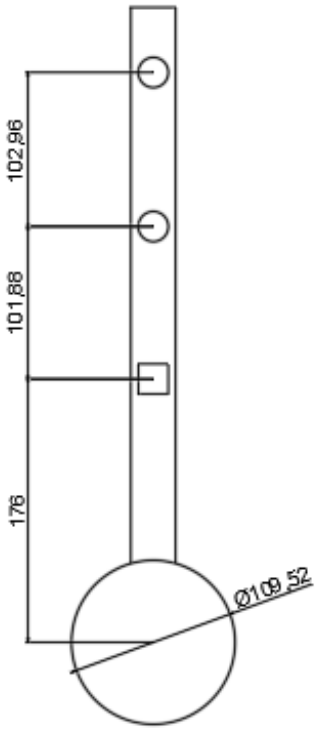

Fig. 3. Distance measurements on the real object.

Table 1. Description of measured parameters

Description	**Index**	**Value**	**Unit**
Distance from reaction wheel center to rotation axis	l_{kz-oo}	176.00	mm
Distance from fixed weight to rotation axis	l_{nc-oo}	101.88	mm
Distance between fixed and movable weights	l_{nc-rc}	102.96	mm
Diameter of the reaction wheel	Φ_{kz}	109.52	mm
Mass of the movable weight	m_{rc}	197.00	g
Total pendulum mass	m_{cw}	69.00	g
Cylinder thickness	h_w	6.32	mm

To verify the total mass of the pendulum, the imbalance value is calculated using the formula:

$$U = m \cdot e \tag{10}$$

where:

- U – Imbalance value,
- e – Eccentricity of the center of mass,
- m – Distance of the reaction wheel center from the rotation axis.

Substituting the values into the formula:

$$U = 0.176 \cdot 0.069 = 0.012144[m \cdot kg]$$

7 Identification of Gravitational Force Torque

To determine the torque due to gravitational force, the imbalance mass of the pendulum was first measured. The pendulum was set horizontally so that $sin(\theta)$ was close to 1. A scale was then placed under the reaction wheel, and the following values were read:

$$M = 0.075\ kg$$

The distance from the center of the reaction wheel to the rotation axis was also measured:

$$L = 0.175\ m$$

Using this information and the gravitational acceleration value, the torque due to gravity was calculated:

$$MgL = 0.129\ kgm^2$$

8 Identification of Friction Coefficient at Pendulum Axis

To identify the friction coefficient at the pendulum's axis of rotation, free damping measurements were conducted. First, measurements were taken for a deflection of 90° and then for 45°. The results are illustrated in Figure 4, and the data is recorded in Table 2.

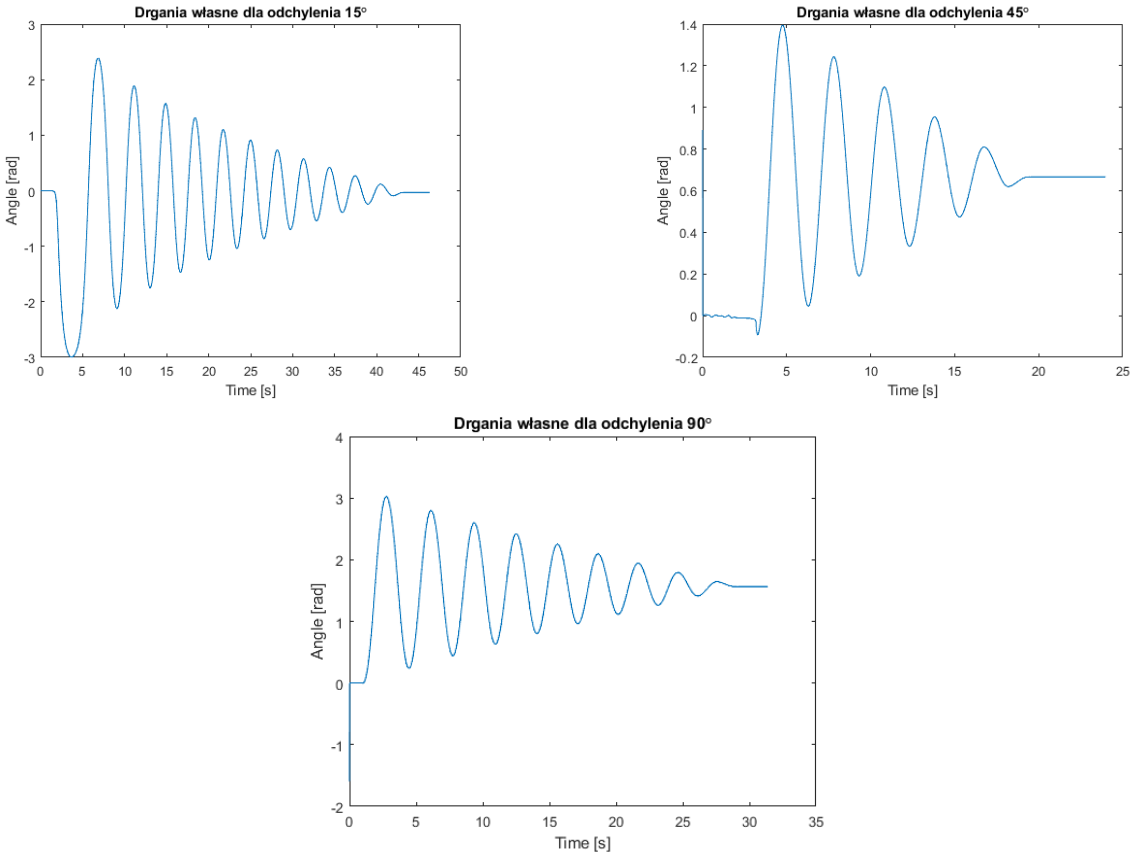

Fig. 4. Measurements of free oscilations

Measurements marked in red were discarded due to excessive deflection angles of the pendulum. This is because the formula used to calculate the oscillation period assumes small deflections. Excessive deflections can lead to uneven durations of single oscillations. Based on the remaining measurements, the average oscillation period was calculated:

$$T = 3.170[s]$$

Table 2. Oscillation period measurements for the pendulum

No	Pendulum Angle	No of Oscillations	Total Oscillation Time	Oscillation Period
1.	45°	4.75	15.36[s]	3.234
2.	45°	4.75	15.35[s]	3.232
3.	45°	4.75	15.01[s]	3.160
4.	45°	4.75	15.21[s]	3.202
5.	90°	9.75	30.21[s]	3.098
6.	90°	9.75	30.68[s]	3.147
7.	−90°	9.25	29.83[s]	3.225
8.	−90°	9.25	29.54[s]	3.190
9.	15°	1.75	5.43[s]	3.103
10.	15°	1.75	5.41[s]	3.091

8.1 Analytical Determination of the Friction Coefficient

Next, the lengths of two consecutive amplitudes were calculated to determine the logarithmic decrement of damping, which is the ratio of two successive amplitudes in damped motion. The decreasing amplitudes are shown below.

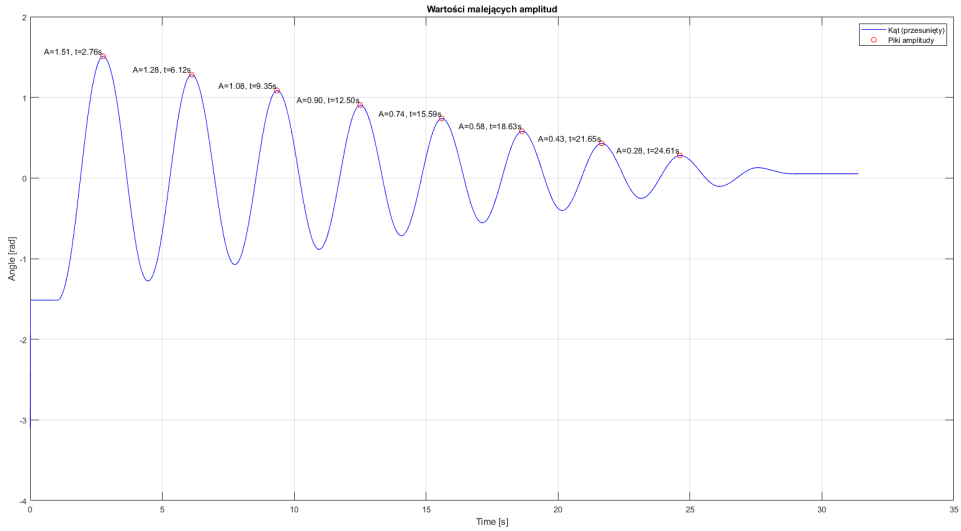

Fig. 5. Damped oscillations with plotted amplitudes.

Subsequent measurements were made and are presented in the table below. The *findpeaks()* function was used to calculate the global maximum values.

Table 3. Amplitude measurements for deflection of 90°.

Measurement	Amplitude A1 [rad]	Amplitude A2 [rad]
1	1.51	1.28

Using this data, the logarithmic decrement of damping for $n = 1$ was calculated:

$$\delta = \ln\left(\frac{A_n}{A_{n+k}}\right) = \ln\left(\frac{A_1}{A_2}\right) = 0.06765 \tag{11}$$

From this information, the damping coefficient was calculated as **0.15700**. Additionally, the curve fitting $A_1 \cdot e^{-\delta t}$ was checked to illustrate whether the coefficient was determined correctly.

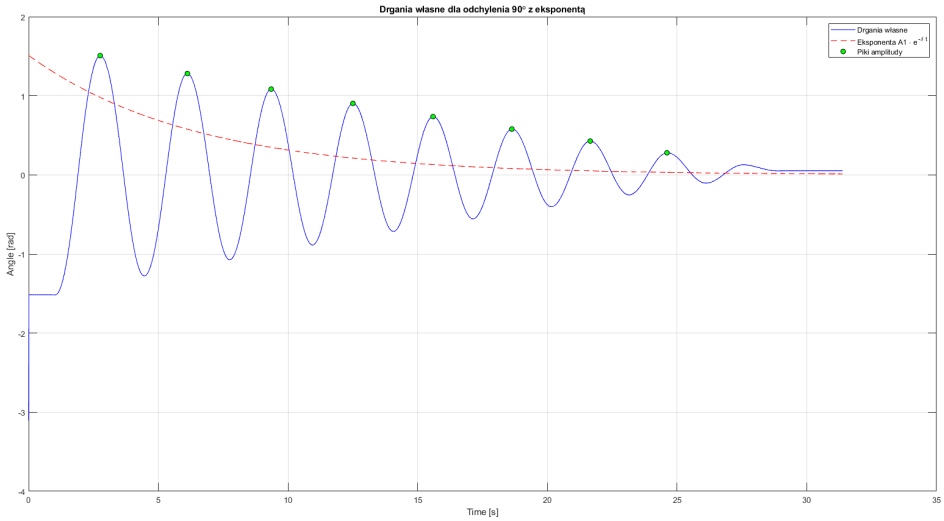

Fig. 6. Damped oscillations with fitted curve for deflection of 90°.

The graph above suggests that the damping coefficient was poorly fitted. The mismatch stems from approximations of amplitude values and working with a nonlinear model. Additional studies of the friction coefficient for deflections of 45° and 15° were also conducted, but the results were discarded due to poor curve fitting. Figures below illustrate this issue.

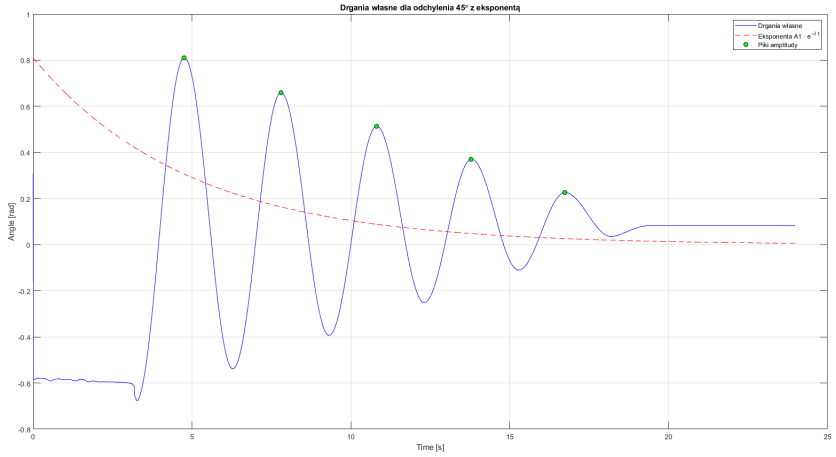

Fig. 7. Damped oscillations with fitted curve for deflection of 45°.

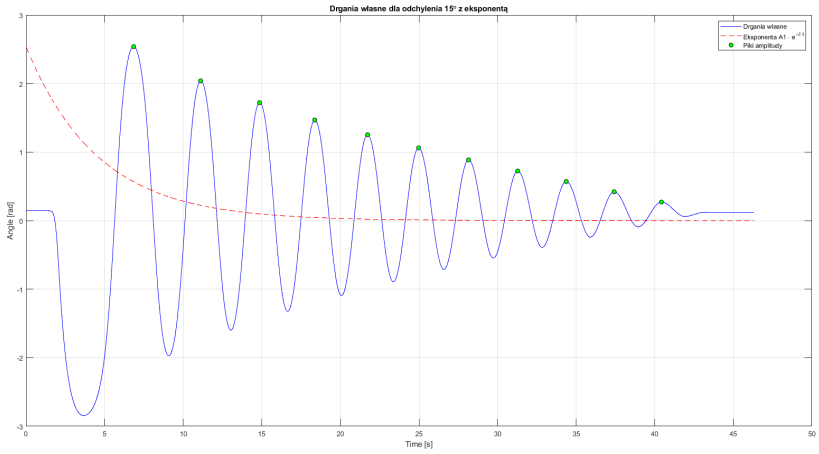

Fig. 8. Damped oscillations with fitted curve for deflection of 15°.

It was concluded that the main reason for the mismatch is the nonlinear behavior of the friction coefficient. Additionally, the changing oscillation period with each deflection complicates the analysis further.

9 Identification of Moment of Inertia

Identifying the moment of inertia required distinguishing between the moment of inertia of the rotor disc, calculated using mathematical relations, and the moment of inertia of the pendulum arm, determined experimentally through free oscillation measurements.

9.1 Determining the Moment of Inertia of the Rotor Disc

The rotor disc was treated as a cylinder made of aluminum. Constants and measured parameters are listed in Table 6.

Table 4. Parameters for calculations

Description	Index	Value	Unit
Height	h	0.0063	[m]
Radius	r	0.0541	[m]
Density	ρ	2700	$[\frac{kg}{m^3}]$

First, the volume of the rotor disc was calculated:

$$V = \pi \cdot r^2 \cdot h \tag{12}$$

Next, the mass:

$$m = \rho \cdot V \tag{13}$$

Finally, the moment of inertia of the rotor disc:

$$J_{rotor} = \frac{1}{2} \cdot m \cdot r^2 \tag{14}$$

The calculation results are summarized in Table 5.

Table 5. Calculated parameters of the rotor disc

Description	Index	Value	Unit
Rotor disc volume	V	$5.802 \cdot 10^{-5}$	$[m^3]$
Rotor disc mass	m	0.157	[kg]
Rotor disc moment of inertia	J_{rotor}	$2.289 \cdot 10^{-4}$	$[kg \cdot m^2]$

9.2 Determining the Moment of Inertia of the Pendulum Arm

To determine the moment of inertia of the pendulum arm, the average period of free oscillation measured during the identification of the friction coefficient was used:

$$T_{osc} = 3.17\ s$$

The moment of inertia of the entire pendulum can be calculated using the following formula:

$$J_{pendulum} = U \cdot g \cdot L \cdot \frac{T_{osc}^2}{4\pi^2} \tag{15}$$

where:

$J_{pendulum}$ –Moment of inertia of the pendulum arm,

U – Imbalance value,
g – Gravitational acceleration,

L – Distance from the rotation axis to the center of mass,
T_{osc} – Average period of free oscillations.

The obtained value is:

$$J_\Theta = 0.0267\ kgm^2$$

10 Determining Friction Coefficient Using *Parameter Estimator*

After analyzing the experiment *"Analytical Determination of the Friction Coefficient"*, it was decided to change the method of determining the friction coefficient.
Friction was divided into kinetic (dynamic) and static friction. Additionally, friction coefficients for the pendulum arm and the rotor disc were treated as separate parameters.
With these assumptions, the friction coefficients were determined.

10.1 Determining Rotor Disc Friction

Rotor disc friction was determined based on motion dynamics:

$$K \cdot \omega = M_{drive} - M_{friction} \tag{16}$$

where:

K – Kinetic friction influence,
ω – Angular velocity,
M_{drive} – Motor drive torque,
$M_{friction}$ –Friction torque of the rotor disc.

$$K = \frac{1}{J_{rotor}} \tag{17}$$

where:

J_{rotor} – Moment of inertia of the reaction wheel.

$$M_{friction} = \mu_v + \text{sgn}(\mu_c) \tag{18}$$

where:

μ_c – Kinetic friction coefficient,
μ_v – Static friction coefficient.

A *Simulink* model was created to represent the motion dynamics equations. Blocks for the initial values of friction coefficients ($\mu_{v,init}$ and $\mu_{c,init}$) were included. Since angular acceleration was measured, angular velocity was represented as the integral of acceleration multiplied by a gain (symbolizing the influence of kinetic friction on the system).

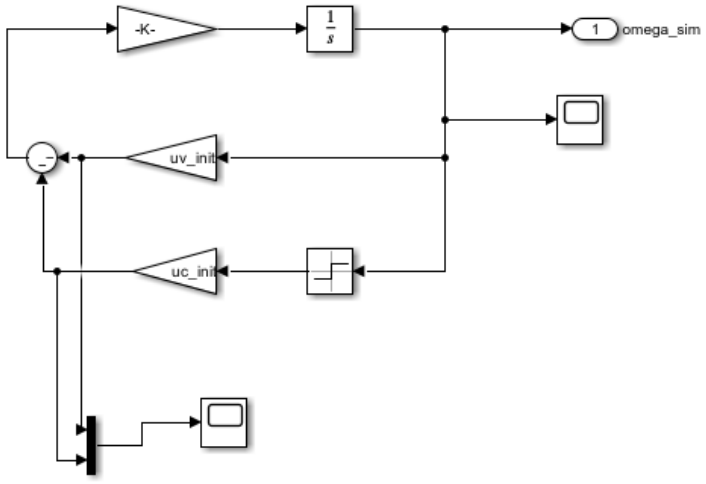

Fig. 9. Model representing motion dynamics equations for determining rotor disc friction.

An experiment was conducted to estimate the kinetic and static friction coefficients, with the results presented in the following figure:

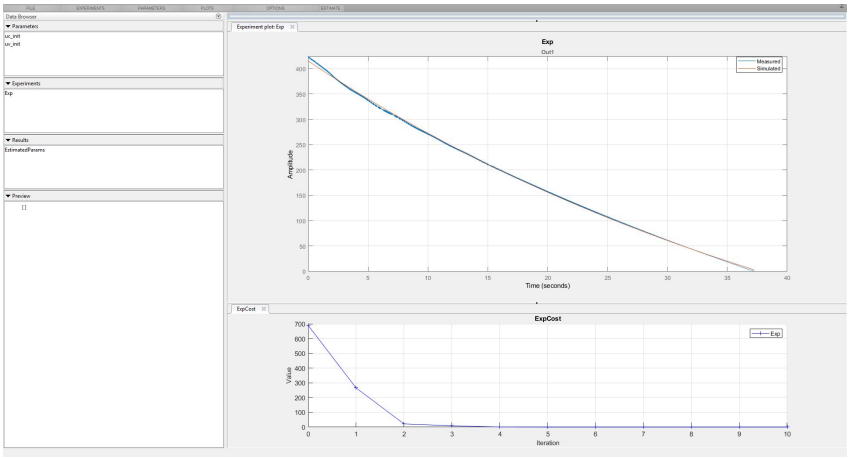

Fig. 10. Parameter estimation for friction coefficients.

10.2 Determining Pendulum Arm Friction

To determine the friction coefficients of the pendulum arm, the above process was repeated, but the model was modified based on the motion dynamics equations. The pendulum dynamics include the gravitational force, so the equations were updated accordingly:

$$K \cdot \omega = M_{drive} - M_{friction} - F_g \tag{19}$$

where:

K – Kinetic friction influence,
ω – Angular velocity,
M_{drive} – Motor drive torque,
$M_{friction}$ –Friction torque,
F_g – Gravitational force.

$$K = \frac{1}{J_{pendulum}} \tag{20}$$

where:

$J_{pendulum}$ –Moment of inertia of the pendulum.

$$F_g = \sin(\theta) \cdot U \cdot g \tag{21}$$

where:

U – Imbalance value,
g – Gravitational acceleration.

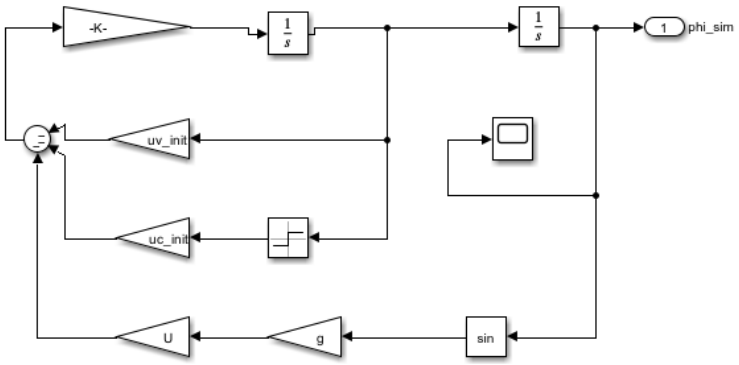

Fig. 11. Model representing motion dynamics equations for determining pendulum arm friction.

Results from these experiments are presented in the table below.

Table 6. Results of friction coefficient determination

Description	**Index**	**Value**
Static friction coefficient of the rotor disc	$\mu_{v,dc}$	$5.302 \cdot 10^{-6}$
Kinetic friction coefficient of the rotor disc	$\mu_{c,dc}$	$1.600 \cdot 10^{-3}$
Static friction coefficient of the pendulum arm	$\mu_{v,pend}$	$1.848 \cdot 10^{-4}$
Kinetic friction coefficient of the pendulum arm	$\mu_{c,pend}$	$4.346 \cdot 10^{-3}$

11 Object Model

Based on the state equations described in the subsection *"Mathematical Model"* and the identification of inertia and friction coefficients, an object model was built in *Simulink*, as shown in Figure 14.

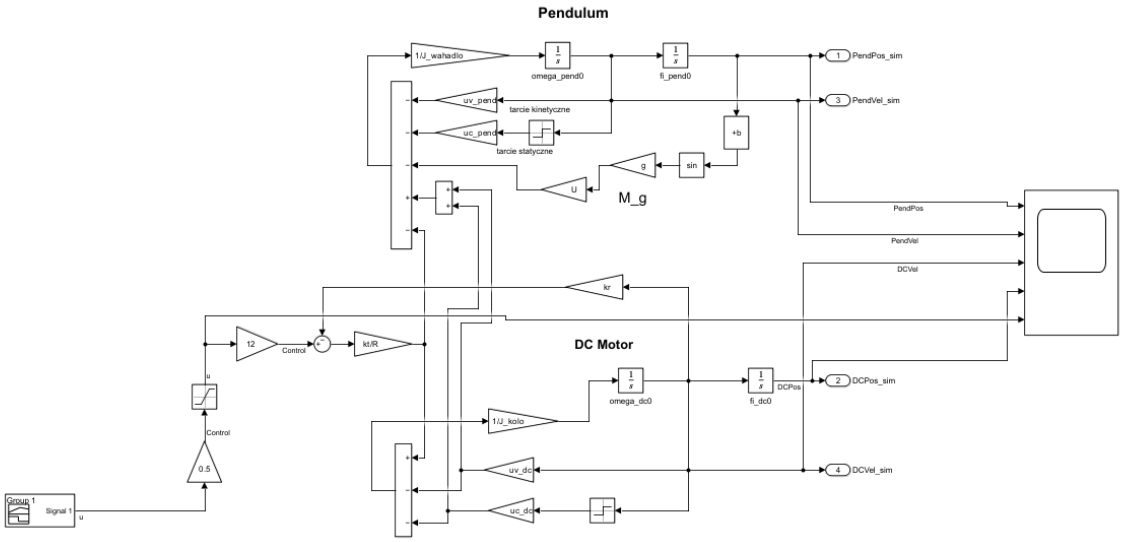

Fig. 12. Object model.

This model was subjected to an unusual control signal (Figure 14) to test the model's response relative to the behavior of the real object.

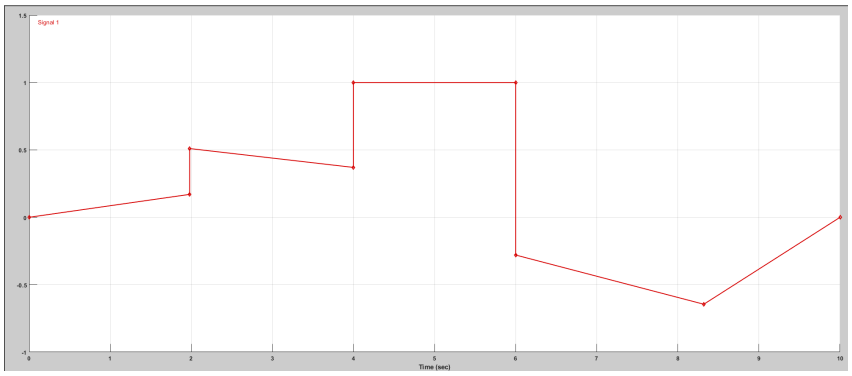

Fig. 13. Control signal.

Data collected from the real object's simulation for the same control signal were loaded into MATLAB's workspace and compared on a single graph for each state variable.

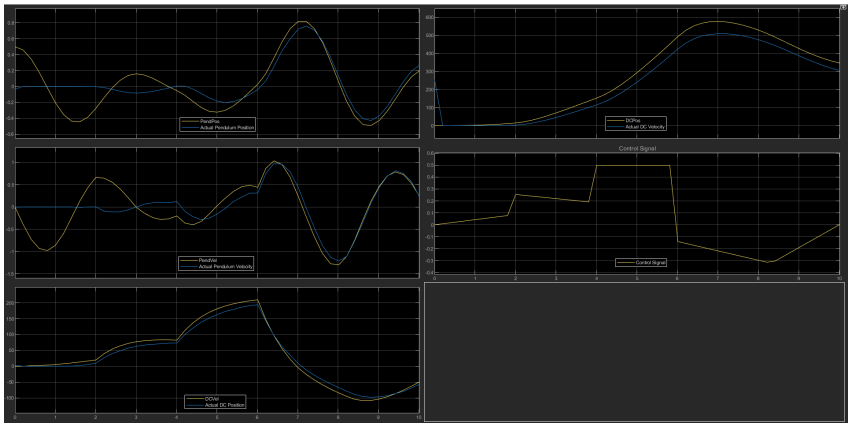

Fig. 14. Comparison of the model's response with the real object.

12 Model Linearization

12.1 Mathematical Approach

To linearize the model, we return to the mathematical description of the motion equations:

$$J_\Theta \ddot{\Theta} = MgLsin(\Theta) - \mu_\Theta \dot{\Theta} + \left(\tau \frac{k_t k_r}{R} + \mu_\varphi\right) \dot{\varphi} - \frac{k_t}{R} u \tag{22}$$

$$J_\varphi \ddot{\varphi} = -\left(\tau \frac{k_t k_r}{R} + \mu_\varphi\right) \dot{\varphi} + \frac{k_t}{R} u \tag{23}$$

Initially, four state variables were proposed, but for controlling pendulum motion in a circular path, only three are necessary. The focus is on the motor speed, which generates the driving torque that moves the pendulum, rather than its position.

$$\begin{cases} x_1 = \theta \\ x_2 = \theta' \\ x_3 = \varphi' \end{cases} \tag{24}$$

The system aims to stabilize the pendulum in the upper position with zero velocities for both the pendulum and the reaction wheel. Thus, the system seeks zero values for the state variables:

$$\begin{cases} x_1 = \theta & = 0 \\ x_2 = \theta' & = 0 \\ x_3 = \varphi' & = 0 \end{cases} \tag{25}$$

The revised state equations are:

$$\begin{cases} {x_1}' = x_2 \\ {x_2}' = \dfrac{1}{J_\Theta}\left(MgL\sin(\Theta) - \mu_\Theta x_2 + \left(\tau \dfrac{k_t k_r}{R} + \mu_\varphi\right) x_3 - \dfrac{k_t}{R} u\right) \\ {x_3}' = \dfrac{1}{J_\varphi}\left(-\left(\tau \dfrac{k_t k_r}{R} + \mu_\varphi\right) x_3 + \dfrac{k_t}{R} u\right) \end{cases} \tag{26}$$

Since the only nonlinearity in these equations is $\sin(\theta)$, it can be approximated as $\sin\theta \sim \theta$ for small deviations near the unstable equilibrium (upper position). The equations then become:

$$\begin{cases} {x_1}' = x_2 \\ {x_2}' = \dfrac{1}{J_\Theta}\left(MgL\Theta - \mu_\Theta x_2 + \left(\tau \dfrac{k_t k_r}{R} + \mu_\varphi\right) x_3 - \dfrac{k_t}{R} u\right) \\ {x_3}' = \dfrac{1}{J_\varphi}\left(-\left(\tau \dfrac{k_t k_r}{R} + \mu_\varphi\right) x_3 + \dfrac{k_t}{R} u\right) \end{cases} \tag{27}$$

From these equations, the system matrices A and B are constructed:

$$A = \begin{bmatrix} 0 & 1 & 0 \\ \frac{mgl}{J_\theta} & -\frac{1}{J_\theta} & \frac{\tau}{J_\theta}\frac{k_t k_r}{R} \\ 0 & 0 & -\frac{\tau}{J_\theta}\frac{k_t k_r}{R} \end{bmatrix} \tag{28}$$

$$B = \begin{bmatrix} 0 \\ -\frac{U k_t}{R J_\phi} \\ \frac{U k_t}{R J_\phi} \end{bmatrix} \tag{29}$$

Substituting parameter values yields:

$$A = \begin{bmatrix} 0 & 1.0000 & 0 \\ 4.4672 & -0.0069 & 0.0108 \\ 0 & 0 & -1.2325 \end{bmatrix} \tag{30}$$

$$B = \begin{bmatrix} 0 \\ -2.4373 \\ 283.9282 \end{bmatrix} \tag{31}$$

$$C = \begin{bmatrix} 1 & 0 & 0 \\ 0 & 1 & 0 \\ 0 & 0 & 1 \end{bmatrix} \tag{32}$$

$$D = \begin{bmatrix} 0 \\ 0 \\ 0 \end{bmatrix} \tag{33}$$

12.2 Linear Analysis Tool

For comparison purposes, linearization was also performed using MATLAB's *Linear Analysis Tool*. Before proceeding, the model was prepared in the following form:

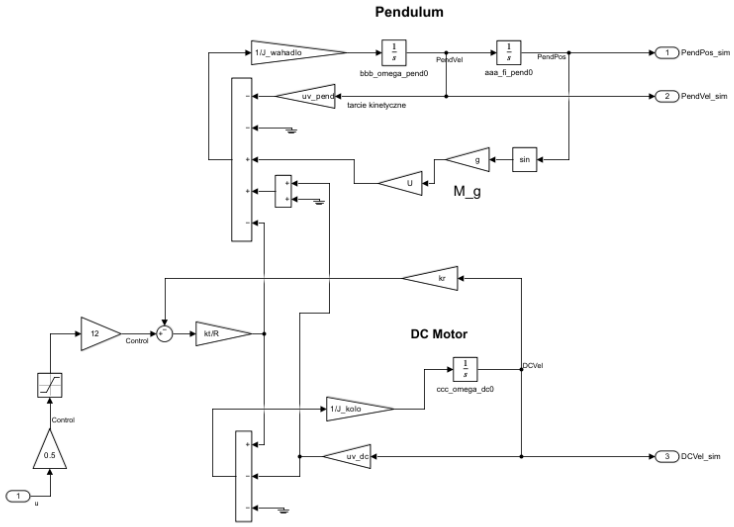

Fig. 15. Model prepared for linearization.

Linearization was conducted based on the step response of the prepared model.

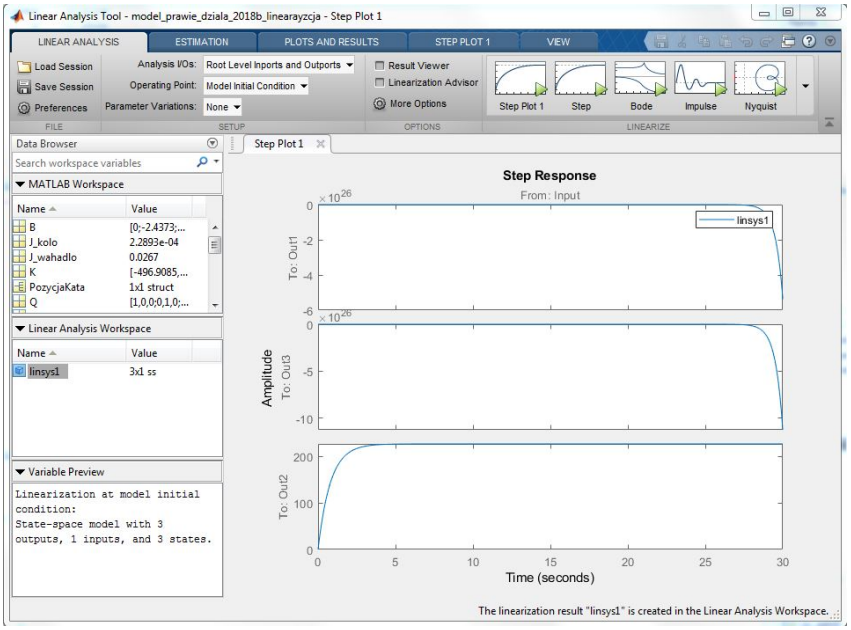

Fig. 16. Linearization using *Linear Analysis Tool*.

The operating point of this system is the previously mentioned upper position of the pendulum, where the values of the state variables are zero. Using the *Linear Analysis Tool*, the following state matrices were obtained:

$$A = \begin{bmatrix} 0 & 1.0000 & 0 \\ 4.4672 & -0.0069 & 0.0108 \\ 0 & 0 & -1.2325 \end{bmatrix} \tag{34}$$

$$B = \begin{bmatrix} 0 \\ -2.4373 \\ 283.9282 \end{bmatrix} \tag{35}$$

$$C = \begin{bmatrix} 1 & 0 & 0 \\ 0 & 1 & 0 \\ 0 & 0 & 1 \end{bmatrix} \tag{36}$$

$$D = \begin{bmatrix} 0 \\ 0 \\ 0 \end{bmatrix} \tag{37}$$

It can be observed that identical values were obtained as with the mathematical method, confirming the correctness of the calculations.

12.3 System Information

First, to obtain information about the linearized model, the eigenvalues of the system were calculated. Based on these, it is possible to determine whether the system is asymptotically stable, stable, or unstable. The calculated eigenvalues are:

$$\text{eigenvalues} = \begin{bmatrix} 2.1101 \\ -2.1170 \\ -1.1535 \end{bmatrix} \tag{38}$$

It can be seen that one of the eigenvalues has a positive value, which means the system in the upper position is unstable. Therefore, to stabilize it in this position, a controller is necessary. The next crucial step is to check the controllability of the system. To verify this property, the controllability matrix was calculated:

$$Q = \begin{bmatrix} 0 & -2.4373 & 3.0721 \\ -2.4373 & 3.0721 & -14.7390 \\ 283.9282 & -355.9079 & 446.1355 \end{bmatrix} \tag{39}$$

The ranks of matrices Q and A are equal, so the system is controllable. Controllability is a property of a dynamic system that determines the ability to influence the system's state through control. A system is controllable if there exists a control that can move the system from any initial state to any final state in a finite amount of time.

Another important property is the observability of the system. To verify this, the observability matrix was first calculated:

$$O = \begin{bmatrix} 1.0000 & 0 & 0 \\ 0 & 1.0000 & 0 \\ 0 & 0 & 1.0000 \\ 0 & 1.0000 & 0 \\ 4.4672 & -0.0069 & 0.0108 \\ 0 & 0 & -1.2535 \\ 4.4672 & -0.0069 & 0.0108 \\ -0.0309 & 4.4672 & -0.0136 \\ 0 & 0 & 1.5713 \end{bmatrix} \tag{40}$$

In this case as well, the ranks of matrices O and A are equal, so the system is observable. Observability is a property that indicates the ability to determine the state of the system based on its output. A system is observable if its state can be uniquely determined from its output over a finite period of time.

13 LQR Controller Design Based on Model Linearization

An LQR controller was designed based on the linearized model obtained using the *Linear Analysis Tool*. The LQR controller is an algorithm for linear systems, minimizing a weighted sum of state errors and control effort. Using MATLAB's *lqr* function, which takes the state matrix A, input matrix B, and weight matrices Q and R, the gain matrix K was computed. Initially, the weight matrices were chosen as follows:

$$Q = \begin{bmatrix} 1 & 0 & 0 \\ 0 & 1 & 0 \\ 0 & 0 & 1 \end{bmatrix}$$

$$R = 1 \tag{41}$$

With these parameters, the gain matrix K was calculated:

$$K = \begin{bmatrix} -196.9085 & -234.7209 & -1.0044 \end{bmatrix} \tag{42}$$

The stability of the closed-loop system was verified by checking the eigenvalues of the dynamic matrix with feedback:

$$A_c = A - B \cdot K \tag{43}$$

The eigenvalues were:

$$\begin{bmatrix} -9.4216 \\ -2.0550 \\ -2.0550 \end{bmatrix} \tag{44}$$

All eigenvalues are negative, confirming the system's stability. The LQR controller was then implemented in *Simulink* for further testing and tuning of the Q and R matrices.

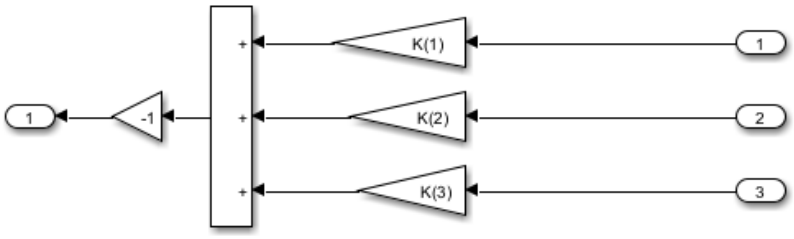

Fig. 17. LQR controller subsystem.

The controller inputs are the pendulum angle, pendulum velocity, and motor velocity.

14 Experimental and Simulation Testing

The next step was testing the designed controller on the system. First, simulations verified the correctness and functionality of the controller. Subsequently, measurements on the real system were used to fine-tune the controller by adjusting the Q and R weight matrices.

14.1 Tuning the LQR Controller's Weight Matrices

Through a series of experiments, individual weights of the Q and R matrices were adjusted, and the system behavior was analyzed to achieve optimal performance. The final values of the weight matrices and gain matrix K were as follows:

$$Q = \begin{bmatrix} 1 & 0 & 0 \\ 0 & 10 & 0 \\ 0 & 0 & 0.01 \end{bmatrix},$$

$$R = 10, \tag{45}$$

$$K = \begin{bmatrix} -19.51 \\ -9.27 \\ -0.036 \end{bmatrix}.$$

15 Performance Indicators

To evaluate the operation of the system with the designed and tuned controller, two integral performance indicators were calculated for various experiments, and the pendulum stabilization time was manually read and analyzed:

- Integral of the squared control error.
- Integral of the absolute control effort multiplied by time.
- Stabilization time.

Three different experiments were conducted. In each, a constant disturbance of the pendulum's deflection from equilibrium by 0.2 rad was introduced every 10 seconds. The first experiment was performed on the model with unchanged parameters. In the second experiment, the weight's distance from the center of rotation was increased to observe the impact of moment of inertia changes on controller performance. The last experiment introduced a constant reaction wheel speed of 100 rad/s. The performance indicator values obtained for the entire duration (20 seconds) are as follows:

- **First Experiment**

- Integral of the squared control error:

  0.4162

- Integral of the absolute control effort multiplied by time:

  8.6199

- Stabilization time:

  none

- **Second Experiment**
  - Integral of the squared control error:

    0.2823

  - Integral of the absolute control effort multiplied by time:

    4.8615

  - Stabilization time:

    none

- **Third Experiment**
  - Integral of the squared control error:

    2.0478

  - Integral of the absolute control effort multiplied by time:

    22.5588

  - Stabilization time:

    none

Below are the control response graphs for each of the three experiments.

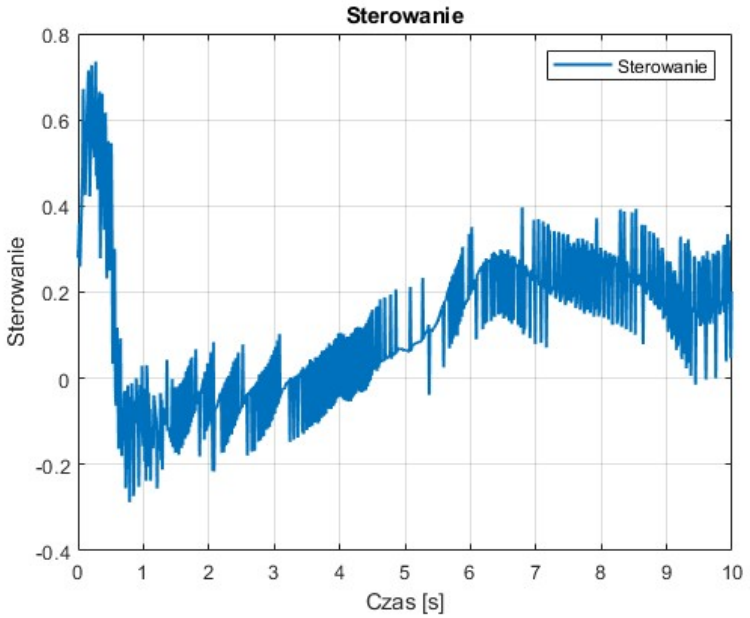

Fig. 18. Control response for the first experiment.

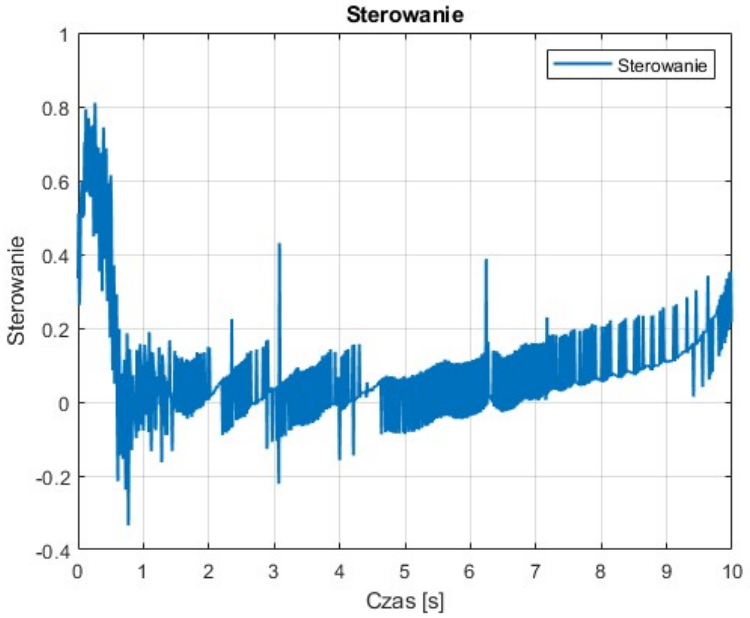

Fig. 19. Control response for the second experiment.

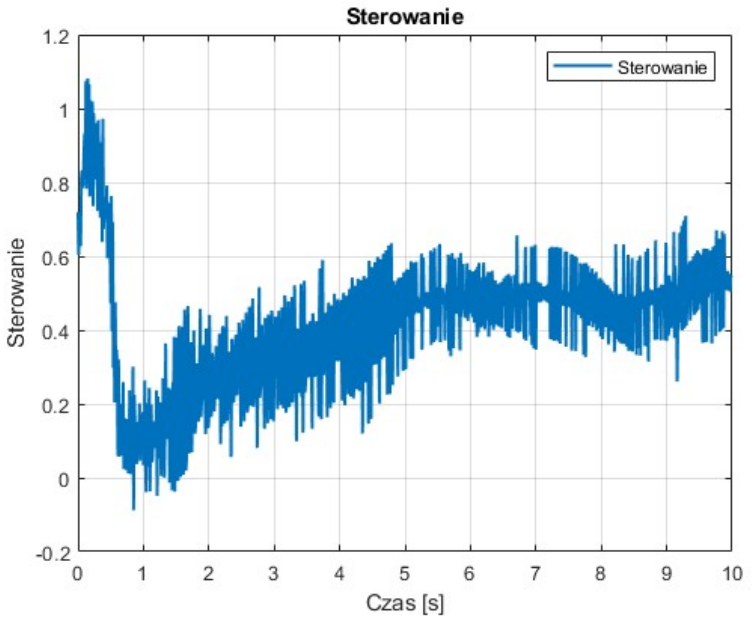

Fig. 20. Control response for the third experiment.

15.1 Conclusions

Due to the frequency of disturbances introduced to the system, it was not possible to precisely determine the stabilization time. The system oscillated around the setpoint without deviating far from it, suggesting that the designed controller could bring the system to equilibrium under any conditions (model parameter changes). Thus, the controller is robust to minor parameter disturbances.

High noise levels in the control signal were observed in each experiment, which is suboptimal controller performance. A positive aspect is the near absence of saturation (control limits between -1 and 1) during the experiments.

16 Summary

The exercises with the reaction pendulum provided comprehensive knowledge in mathematical modeling, parameter identification, and control method design and implementation. Analyzing the system, which is an example of an unstable nonlinear system, allowed for a better understanding of the complex interactions between system elements and the influence of physical parameters on system dynamics.

Key takeaways include: - Accurate parameter identification, including moments of inertia, friction coefficients, and gravity-related parameters. - Development of a mathematical model based on Newtonian dynamics, sufficiently detailed for building simulations in MATLAB Simulink. - Successful linearization, both analytically and using MATLAB's *Linear Analysis Tool*, enabling simplified controller design.

The designed LQR controller effectively stabilized the pendulum in the upright position, even though the system is naturally unstable in this state. Fine-tuning of the Q and R matrices improved control quality under experimental conditions. Despite minor limitations such as noise and oscillations near equilibrium, the results confirm the controller's robustness and effectiveness.

This project provided valuable experience in modeling and controlling complex dynamic systems, laying a solid foundation for future applications in more advanced and practical scenarios.

References

[1] „*Reaction Wheel Pendulum*". https://www.inteco.com.pl/products/reaction-wheel-pendulum/. Access: 2024-03-02.